Phase-field simulations of stress-strain behavior in ferromagnetic shape memory alloy Ni_2MnGa

P. P. Wu,[1,a)] X. Q. Ma,[1] J. X. Zhang,[2] and L. Q. Chen[2]
[1]*Department of Physics, University of Science and Technology Beijing, Beijing 100083, China*
[2]*Department of Material Science and Engineering, The Pennsylvania State University, University Park, Pennsylvania 16802, USA*

(Received 29 January 2008; accepted 12 August 2008; published online 7 October 2008)

The evolution of strain, magnetic domain structure, and martensite microstructure during compressive stress loading and unloading of Ni_2MnGa was studied using a phase-field model at several selected magnetic fields. We observed a typical quasiplastic behavior at zero field and a pseudoelastic behavior at 300 kA/m. At an intermediate field, 150 kA/m, the stress-strain relation is partially pseudoelastic. It was demonstrated that the magnetic domain structure has little influence on the recovered strain while the demagnetization factor impacts the strain reversal. © *2008 American Institute of Physics*. [DOI: 10.1063/1.2988898]

I. INTRODUCTION

Ni_2MnGa is a ferromagnetic shape memory alloy (FSMA) that can generate large strains using a magnetic field. Since its discovery by Ullakko *et al.*[1] in 1996, Ni_2MnGa has been shown to produce up to 6% strains for alloys containing tetragonal martensite and 10% with orthorhombic martensite.[2,3] It has been extensively studied due to its potential applications in actuators and sensors, particularly in actuating applications that require large motions.

There have been a number of prior studies on the stress-strain behaviors of Ni_2MnGa. For example, Müllner *et al.*[4] first studied the reversible (pseudoelastic) stress-strain behavior of single crystal Ni_2MnGa at a constant magnetic field of 558 kA/m. They reported that the stress-strain curve shows a wide hysteresis whereas the strain-magnetization hysteresis is narrow. Straka and Heczko[5] and Heczko[6] established a direct relation between magnetization (M) and strain (ε) by measuring them simultaneously and by using a simple energy model. Likhachev *et al.*[7] performed mechanical testing experiments in three types of martensitic phases of Ni_2MnGa (5M, 7M, and NM) and observed the pseudoelastic behavior during loading and unloading under a magnetic field of about 1 T. Recently, a behavior named partial pseudoelastic recovery was also observed.[8–10] Sarawate and Dapino[8,9] showed some detailed experiment results and developed a thermodynamics model to describe a transition from being quasiplastic to pseudoelastic in Ni_2MnGa single crystals under different applied external magnetic fields. A quasistatic model, developed by Couch and Chopra,[10] was also used to explain the quasiplastic, pseudoelastic, and partial pseudoelastic processes at different applied fields. It should be pointed out that due to its ferromagnetic nature, magnetization in Ni_2MnGa alloy is strongly dependent on its magnetization history and thermal pretreatment. For example, Li *et al.*[11] observed some distinctly different magnetization processes of a Ni_2MnGa single crystal after different magnetic and thermal pretreatments.

In this paper, we employed a phase-field method[12] to study the quasiplastic and pseudoelastic processes. The main advantage over previous theoretical works is the fact that it allows one to examine in detail the evolution of domain structure and martensitic twin microstructure under combined applied mechanical and magnetic fields. We determine the stress-strain curve and the magnetization-strain curve in a single crystal Ni_2MnGa under different applied external magnetic fields. The influence of applied magnetic fields and domain structures on the recovery strain was also investigated. We showed that the applied field plays a major role in the strain recovery while the domain structure only has small influence on the reversible strain.

II. PHASE-FIELD MODEL

In our phase-field model, a given microstructure state of FSMA is described by two fields: a local magnetization field, $M(r)$, and a stress-free transformation strain field, ε_{ij}^o. While the magnetization field describes the magnetic domain structure, the stress-free strain field specifies the martensite microstructure.

The total free energy of FSMA containing inhomogeneous microstructures is given by

$$E = E_{\text{anis}} + E_{\text{exch}} + E_{\text{ms}} + E_{\text{external}} + E_{\text{Landau}} + E_{\text{gradient}} + E_{\text{me}} + E_{\text{elastic}}, \quad (1)$$

where E_{anis}, E_{exch}, E_{ms}, E_{external}, E_{Landau}, E_{gradient}, E_{me}, and E_{elastic} are the magnetocrystalline anisotropy, magnetic exchange, magnetostatic, Zeeman, Landau, strain gradient, magnetoelastic, and elastic energies, respectively.

As in any Landau-type description of thermodynamics of a phase transition, all energy terms are assumed to have the symmetry of the parent phase. The parent phase of Ni_2MnGa is a cubic phase, and therefore all terms including the magnetocrystalline anisotropy and elastic constants have the cubic symmetry. In the martensite phase, the magnetocrystalline anisotropy energy includes both austenite magnetoanisotropy and the magnetoelastic contribution and thus has the tetragonal symmetry.

a)Electronic mail: pingpingwu-ustb@126.com.

The anisotropy energy of a cubic magnetic crystal is

$$E_{\text{anis}} = \int [K_1(m_1^2m_2^2 + m_1^2m_3^2 + m_2^2m_3^2) + K_2m_1^2m_2^2m_3^2]dV, \tag{2}$$

where K_1 and K_2 are the anisotropy constants and m_i are the components of the unit magnetization vector, $m=M/M_s$, M_s is the saturation magnetization.

The exchange energy in micromagnetism is usually written in the form

$$E_{\text{exch}} = A\int (\text{grad } \boldsymbol{m})^2 dV, \tag{3}$$

where A is the exchange stiffness constant.

The magnetostatic energy of a system can be written as

$$E_{\text{ms}} = -1/2\mu_0 M_s \int \boldsymbol{H}_d \cdot \boldsymbol{m} dV, \tag{4}$$

where μ_0 is the permeability of the vacuum and $\boldsymbol{H}_d$ is the demagnetization field that is determined by the long-range interactions among the magnetic moments in the system.

In this work, we separate the local magnetization field $M(\mathbf{r})$ as a sum of the spatially independent average magnetization part $\bar{M}$ and the spatially dependent heterogeneous part δM. The local magnetic field induced by heterogeneous part δM is calculated by solving Maxwell's equation $H_{d1,1}+H_{d2,2}+H_{d3,3}=-M_s(m_{1,1}+m_{2,2}+m_{3,3})$; the comma in a subscript stands for spatial differentiation, for example, $H_{d1,1}$ stands for $\partial H_1/\partial x_1$ here. The demagnetization field caused by average magnetization is approximately calculated by

$$H_d(\bar{M}) = N\bar{M}, \tag{5}$$

where N is the demagnetization factor, which depends on the shape of the material. The detail about the calculation of the demagnetization field was given in Ref. 13.

The Zeeman energy is taken into account through the interaction between the magnetization and the external field,

$$E_{\text{external}} = -\mu_0 M_s \int \boldsymbol{H}_{\text{ex}} \cdot \boldsymbol{m} dV. \tag{6}$$

The Landau free energy describing the proper martensitic transformation is given in Refs. 14–16.

$$E_{\text{Landau}} = \int [Q_1e_1^2 + Q_2(e_2^2+e_3^2) + Q_3e_3(e_3^2-3e_2^2) + Q_4(e_2^2+e_3^2)^2 + Q_5(e_4^2+e_5^2+e_6^2)]dV, \tag{7}$$

where Q_1, Q_2, and Q_5 are bulk, deviatoric, and shear moduli, respectively. Q_3 and Q_4 denote third and fourth-order elastic constants. Q_2 is related to temperature T and martensite transformation temperature T_M by $Q_2=Q_{20}(T-T_M)/T_M$. e_i are the symmetry-adapted strain defined in terms of the transformation strains as Ref. 14:

$$e_1 = (\varepsilon_{11}^0 + \varepsilon_{22}^0 + \varepsilon_{33}^0)/\sqrt{3}, \quad e_4 = \varepsilon_{23}^0,$$

$$e_2 = (\varepsilon_{11}^0 - \varepsilon_{22}^0)/\sqrt{2}, \quad e_5 = \varepsilon_{13}^0,$$

$$e_3 = (2\varepsilon_{33}^0 - \varepsilon_{22}^0 - \varepsilon_{11}^0)/\sqrt{6}, \quad e_6 = \varepsilon_{12}^0. \tag{8}$$

Since a cubic to tetragonal martensitic transition was studied here, we set $\varepsilon_{23}^0=\varepsilon_{13}^0=\varepsilon_{12}^0=0$ for simplicity.

The energy contribution of a wall between two tetragonal variants (twin boundary) is introduced through gradients of the order parameters

$$E_{\text{gradient}} = \int \{1/2g[(\varepsilon_{11,1}^0)^2 + (\varepsilon_{11,2}^0)^2 + (\varepsilon_{11,3}^0)^2 + (\varepsilon_{22,1}^0)^2 + (\varepsilon_{22,2}^0)^2 + (\varepsilon_{22,3}^0)^2 + (\varepsilon_{33,1}^0)^2 + (\varepsilon_{33,2}^0)^2 + (\varepsilon_{33,3}^0)^2]\}dV, \tag{9}$$

where g is the strain gradient coefficient.

For a cubic system, the magnetoelastic energy is given by

$$E_{\text{me}} = \int \{B[\varepsilon_{11}^0(m_1^2 - 1/3) + \varepsilon_{22}^0(m_2^2 - 1/3) + \varepsilon_{33}^0(m_3^2 - 1/3)]\}dV, \tag{10}$$

where B is the magnetoelastic coefficient which is a measure of degree of coupling between strain and magnetization.

If we assume that the interfaces developed during microstructure evolution are coherent, elastic strains e_{ij} and thus elastic energy E_{elastic} are generated,

$$e_{ij} = \varepsilon_{ij} - \varepsilon_{ij}^0, \tag{11}$$

where ε_{ij} is the total strain. The corresponding elastic energy can be expressed as

$$E_{\text{elastic}} = \int 1/2c_{ijkl}e_{ij}e_{kl}dV = \int 1/2c_{ijkl}(\varepsilon_{ij} - \varepsilon_{ij}^0)(\varepsilon_{kl} - \varepsilon_{kl}^0)dV, \tag{12}$$

where c_{ijkl} is the second-order elastic stiffness tensor. The summation convention for the repeated indices is employed and $i, j, k, l=1,2,3$.

The temporal evolution of the magnetization configuration, thus the domain structure, is described by the Landau–Lifshitz–Gilbert (LLG) equation

$$(1+\alpha^2)\frac{\partial \boldsymbol{M}}{\partial t} = -\gamma_0 \boldsymbol{M} \times \boldsymbol{H}_{\text{eff}} - \frac{\gamma_0 \alpha}{M_s}\boldsymbol{M} \times (\boldsymbol{M} \times \boldsymbol{H}_{\text{eff}}), \tag{13}$$

where γ_0 is the gyromagnetic ratio, α is the damping constant, and H_{eff} is the effective magnetic field

$$\boldsymbol{H}_{\text{eff}} = -\frac{1}{\mu_0}\frac{\partial E}{\partial \boldsymbol{M}}. \tag{14}$$

The temporal martensitic microstructure evolution is described by the time-dependent Ginzburg–Landau (TDGL) equations

$$\frac{\partial \varepsilon_{ii}^0(x,t)}{\partial t} = -L\frac{\delta E}{\delta \varepsilon_{11}^0}, \tag{15}$$

where L is the kinetic coefficient.

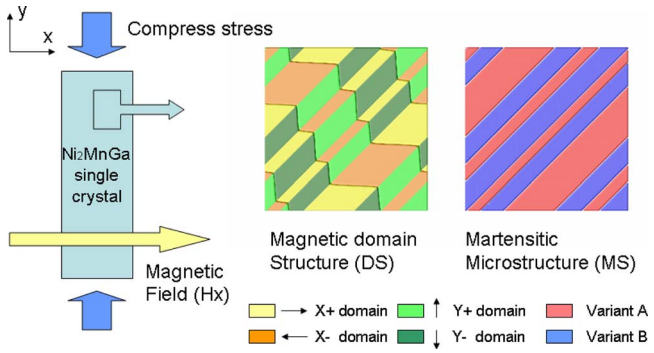

FIG. 1. (Color online) A general schematic of the magnetomechanical setup and the 2D simulation of the magnetic domain structure (DS) and martensitic microstructure (MS) without applying any external field. The magnetic field and the stress field will be added in our simulation, following the directions in the schematic.

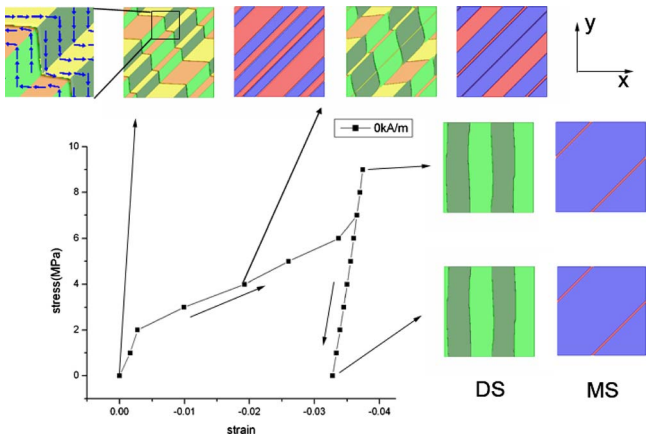

FIG. 2. (Color online) The strain-stress curve of Ni_2MnGa at zero applied field (DS, domain structure; MS, martensite structure). Inset shows a vector map of the initial magnetic domain structure.

III. RESULTS AND DISCUSSION

The parameters of Ni_2MnGa employed in our model are from Refs. 17 and 18: $M_s=6.02\times10^5$ A m^{-1}, $K_1=2.7\times10^3$ J m^{-3}, $K_2=-6.1\times10^3$ J m^{-3}, and $A=2\times10^{-11}$ J m^{-1}. Here we considered that the sample in our work is a sheet that is suitable for two-dimensional (2D) simulations, so we set the demagnetization factor $N_x=N_y=0.02$ and $N_z=0.96$. The coefficients in the Landau free energy and the magnetoelastic coefficient were obtained by fitting the experimental measurements,[17,19] i.e., $Q_1=2.32\times10^{11}$ J m^{-3}, $Q_{20}=3.78\times10^8$ J m^{-3}, $Q_3=0.40\times10^{10}$ J m^{-3}, $Q_4=7.50\times10^{10}$ J m^{-3}, and $B=4.00\times10^6$ J m^{-3}. Martensitic transformation temperature of a defect-free crystal is $T_M^o=300$ K. For a bulk tetragonal Ni_2MnGa crystal, the elastic constants are $c_{11}=1.70\times10^{11}$ N m^{-2}, $c_{33}=1.50\times10^{11}$ N m^{-2}, $c_{12}=1.50\times10^{11}$ N m^{-2}, $c_{13}=1.54\times10^{11}$ N m^{-2}, $c_{44}=0.40\times10^{11}$ N m^{-2}, and $c_{66}=0.45\times10^{11}$ N m^{-2}.[20] In order to avoid solving an elastic equation with inhomogeneous modulus, we choose c_{11} as the average of c_{11} and c_{33}, c_{12} the average of c_{12} and c_{13}, and c_{44} the average of c_{44} and c_{66}, i.e., $c_{11}=1.60\times10^{11}$ N m^{-2}, $c_{12}=1.52\times10^{11}$ N m^{-2}, and $c_{44}=0.43\times10^{11}$ N m^{-2}. In this work, we solved the LLG equation employing the Gauss–Seidle projection method[21] and TDGL equation using the semi-implicit Fourier-spectral method.[22] We employed $256\times256\times1$ discrete cells. Periodic boundary conditions are applied along the x, y, and z axes. The time step for integration is $\Delta t/t_o=0.1$, where $t_o=(1+\alpha^2)/(\gamma_o M_s)$. The cell size, Δx, is 18 nm. The initial condition was created by assigning random orientation for the magnetization and a zero value plus a small random noise for the martensite strain order parameters.

As shown in Fig. 1, a magnetic field is applied on a Ni_2MnGa single crystal sample along the x axis, while the stress field is applied along the y axis, i.e., the magnetic field is provided perpendicular to the loading direction. We first performed phase-field simulations to generate a microstructure with both magnetic domains and martensites without applying a magnetic or stress field. Due to the 2D nature, there are two kinds of martensite variants (variants A and B). Within each martensitic plate, there are magnetic domains separated by 180° domain walls. An example of a microstructure containing two martensite variants and four types of magnetic domains is shown in Fig. 1. A magnetization vector map is shown as an inset in Fig. 2, which illustrates the directions of local magnetization and the "staircaselike" magnetic domain pattern.

It is known that if there is no applied external magnetic field, a Ni_2MnGa single crystal shows a quasiplastic stress-strain behavior, i.e., the deformation will not return to the original shape after the removal of the applied stress. As shown in Fig. 2, a stress was applied along the y axis gradually without an applied magnetic field. The loading process of the quasiplastic behavior can be separated into two stages. At the first stage, the strain change is small as the applied stress increases, and there is no significant magnetic domain wall or martensite twin boundary motion. As the applied stress field increases further, the loading curve reaches the second stage during which the strain climbs up quite rapidly. In this stage the martensite variant B, which is favored by the applied stress field, grows continuously at the expense of variant A through the twin boundary movement. In the corresponding magnetic domain structure, the 90° domain walls between the x domains and the y domains also move accompanying the twin boundary motion. However, the 180° magnetic domain walls within each martensite twin variant show little migration. Further increase in stress (greater than 7 MPa) leads to a single martensite variant with stripe magnetic domains. In such a single martensite variant state, the strain shows a very small change from the elastic deformation of the material. Since we did not add any defect or nucleation mechanism in our simulation, a small amount of minority variant A is retained to facilitate the nucleation and growth of variant A in variant B for the following unloading process.

When the stress is unloaded, the martensite remains as a single variant since there is no driving force for nucleating a new variant. As a result, the strain will not be reversed except for the elastic deformation. In addition, there is no noticeable change in the magnetic domain structure throughout the unloading process.

For a comparison, the pseudoelastic curve under an applied magnetic field of 300 kA/m is shown in Fig. 3(a), with

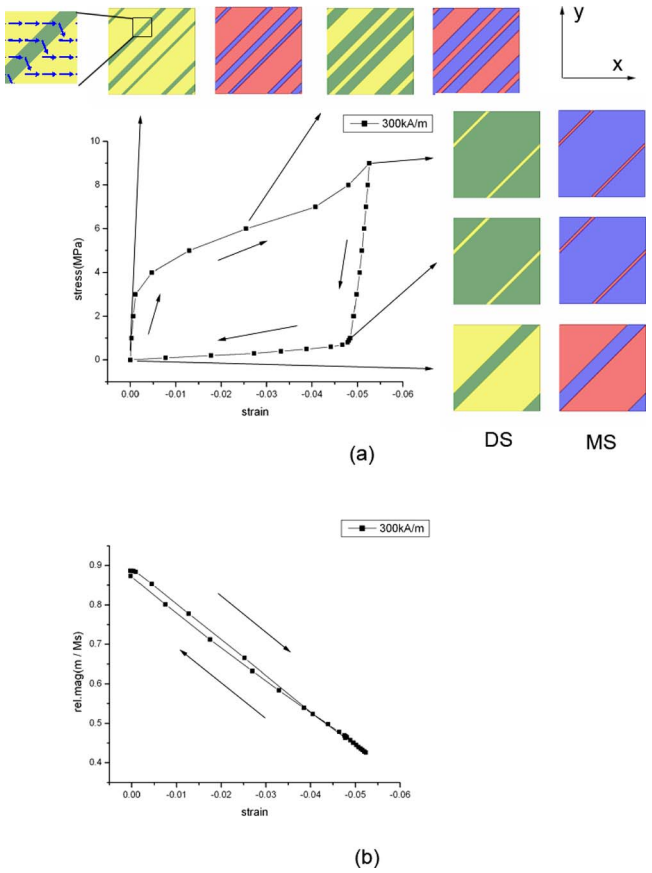

FIG. 3. (Color online) (a) The stress-strain curve of Ni_2MnGa at a magnetic field of 300 kA/m (DS, domain structure; MS, martensite structure). Inset shows a vector map of the initial magnetic domain structure. (b) The strain-magnetization curve in the same processing, showing a narrow hysteresis.

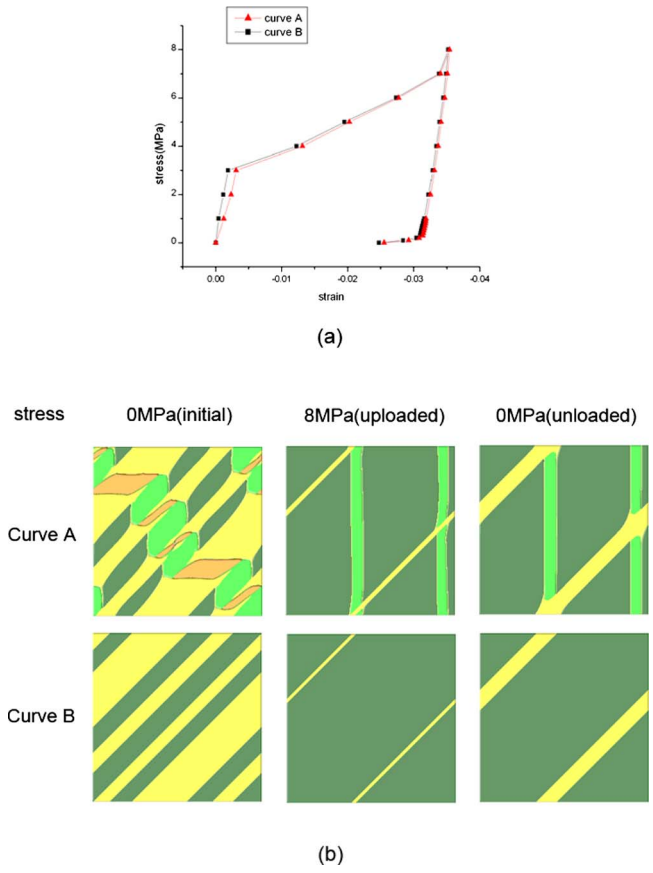

FIG. 4. (Color online) (a) The stress-strain curve of Ni_2MnGa at a field of 150 kA/m. Curves A and B stand for different domain structures. (b) Left: the initial domain structures in curves A and B without stress fields; middle: the two domain structures with an 8 MPa compressive stress; right: the two unloaded domain structures.

the details of the domain structures and martensitic microstructures. We observed that within each martensite variant, the original domain walls disappeared and were replaced by a single magnetic domain after applying under the magnetic field. As a result, there are no 180° domain walls in the domain structure, and only 90° magnetic domain walls coincide with the martensite twin boundaries. During the loading process, the evolution of martensite microstructure is exactly the same as the case with no external applied field discussed above, except that larger applied stress is needed to move the martensite twin boundary due to the presence of the magnetic field. We also observed that the initial slope of Fig. 3 is larger than that of Fig. 2. The increase in the slope is due to the magnetization rotation in variant B (shown in the inset of Fig. 3). The magnetization rotation is not observed in the case with no applied magnetic field (in the inset of Fig. 2). Because of the interactions between the magnetic domains and the martensite variants, the rotation of the magnetization leads to a decrease in the magnitude of strain.

At the end of the loading process, we also left a small amount of variant A to facilitate its nucleation and growth in the unloading process. During the unloading stage, the strain decreases slowly at first as the applied stress magnitude is lowered. Within this stage, the domain structure and the martensite microstructure have no significant changes, similar to the case with no applied field; the slight drop in strain origins from the recovery of elastic deformation. For example, under a stress of 0.8 MPa, the strain only decreases by 0.3%. However, when the applied stress is decreased to below 0.8 MPa, the strain descends rapidly following the reduction in the stress. As shown in Fig. 3, the *x* magnetic domain expanded under the external applied magnetic field, and the martensite twin boundary also started to move as a result of the magnetoelastic coupling effect, leading to the recovery of strain to its original state. Also, throughout the loading and unloading process, the magnetic domain structure and the martensite microstructure closely follow each other, so the relative-magnetization-strain curve shows a narrow hysteresis [as shown in Fig. 3(b)], which is in good agreement with existing experimental results.

From the observed observations, we can see that the pseudoelastic stress-strain behavior will appear when the external magnetic field is large enough to move the martensite twin boundary. However, recent experimental results[8,10] show a partial pseudoelastic behavior at low magnetic fields, while its origin is still not fully understood. We observed similar stress-strain behavior in our simulations, as shown in Fig. 4(a). Under an applied 150 kA/m magnetic field, we first increased the compressive stress to 8 MPa, and then removed it. We noticed that 0.991% strain is recovered according to the hysteresis loop. It was noted that, the corresponding domain structures in curve A has a stripe domain [Fig. 4(b)]

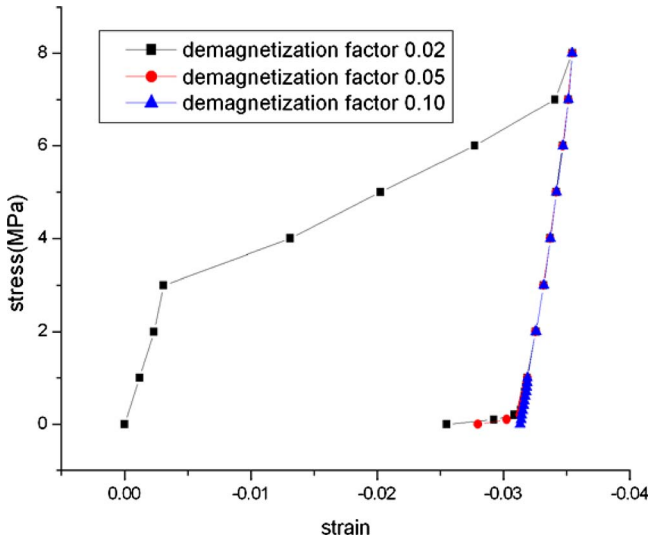

FIG. 5. (Color online) The unloading curves simulated at three different demagnetization factors under a magnetic field of 150 kA/m.

while in our previous simulation results under an applied field of 300 kA/m, there were no 180° domain walls. In order to investigate the influence of the domain structure on stress-strain behavior, we increased the applied field to 170 kA/m, and then decreased it back to 150 kA/m, so a new domain structure with no 180° domain wall was obtained [Fig. 4(b)]. A stress-strain loop with the new domain structure is also shown in Fig. 4(a) as curve B. Compared to the original stress-strain curve, curve B only exhibits a 1.048% recovered strain, which is only about 0.05% higher than the previous recovered strain. The simulation results show that the magnetic domain structure only has little influence on the strain recovery.

Therefore, the partial recovery of the strain is highly related to the magnitude of the applied magnetic field, i.e., when the applied magnetic is small, the demagnetization field may reduce the fully recovery of the strain. To test it, we performed two sets of simulations for the unloading process with different demagnetization factors ($N_x=N_y=0.05$, $N_z=0.90$ and $N_x=N_y=0.10$, $N_z=0.80$). The recovery curves of all the three demagnetization factors are shown in Fig. 5. With the increase in the demagnetization factor, the recovered strain obviously decreases due to the larger demagnetization field.

IV. CONCLUSION

We simulated the loading and unloading of FSMA Ni_2MnGa under different external applied magnetic fields. We analyzed the evolution of magnetic domain structures and martensite structures during the entire loading and unloading process. Three kinds of behavior, the quasiplastic, the pseudoelastic, and the partial pseudoelastic stress-strain behaviors, are observed in our simulation, depending on the magnitude of the applied magnetic field. It is shown that a higher applied magnetic field facilitates the strain reversal, while the magnetic domain structure has little influence on the strain recovery. During the strain recovery process, we observed the 90° magnetic domain wall movement accompanying the variant boundary motion. We also demonstrated that the demagnetization factor influences the magnitude of strain reversal.

ACKNOWLEDGMENTS

This work was supported by the Joint Research Fund for Overseas Chinese Young Scholars from the National Science Foundation of China (Contract No. 50428101).

[1] K. Ullakko, J. K. Huang, C. Kantner, R. C. O'Handley, and T. A. Lograsso, Appl. Phys. Lett. **69**, 1966 (1996).
[2] A. Sozinov, A. A. Likhachev, and K. Ullakko, Proc. SPIE **4333**, 189 (2001).
[3] A. Sozinov, A. Likhachev, N. Lanska, and K. Ullakko, Appl. Phys. Lett. **80**, 1746 (2002).
[4] P. Müllner, V. Chernenko, and G. Kostorz, Scr. Mater. **49**, 129 (2003).
[5] L. Straka and O. Heczko, J. Magn. Magn. Mater. **290–291**, 829 (2005).
[6] O. Heczko, J. Magn. Magn. Mater. **290–291**, 787 (2005).
[7] A. A. Likhachev, A. Sozinov, and K. Ullakko, Mater. Sci. Eng., A **378**, 513 (2004).
[8] N. Sarawate and M. Dapino, Appl. Phys. Lett. **88**, 121923 (2006).
[9] N. N. Sarawate and M. J. Dapino, J. Appl. Phys. **101**, 123522 (2007).
[10] R. N. Couch and I. Chopra, Smart Mater. Struct. **16**, S11 (2007).
[11] G. Li, Y. Liu, and B. K. A. Ngoi, Scr. Mater. **53**, 829 (2005).
[12] J. X. Zhang and L. Q. Chen, Philos. Mag. Lett. **85**, 533 (2005).
[13] J. X. Zhang and L. Q. Chen, Acta Mater. **53**, 2845 (2005).
[14] A. N. Vasil'ev, A. D. Bozhko, V. V. Khovailo, I. E. Dikshtein, V. G. Shavrov, V. D. Buchelnikov, M. Matsumoto, S. Suzuki, T. Takagi, and J. Tani, Phys. Rev. B **59**, 1113 (1999).
[15] A. E. Jacobs, S. H. Curnoe, and R. C. Desai, Phys. Rev. B **68**, 224104 (2003).
[16] J. K. Liakos and G. A. Saunders, Philos. Mag. A **46**, 217 (1982).
[17] R. Tickle and R. D. James, J. Magn. Magn. Mater. **195**, 627 (1999).
[18] D. I. Paul, J. Marquiss, and D. Quattrochi, J. Appl. Phys. **93**, 4561 (2003).
[19] N. Glavatska, G. Mogilniy, I. Glavatsky, S. Danilkin, D. Hohlwein, A. Beskrovnij, O. Söderberg, and V. K. Lindroos, J. Phys. IV **112**, 963 (2003).
[20] L. Dai, J. Cullen, J. Cui, and M. Wuttig, Mater. Res. Soc. Symp. Proc. **785**, D 2.2 (2004).
[21] X. P. Wang and C. J. Garcia-Cervera, J. Comput. Phys. **171**, 357 (2001).
[22] L. Q. Chen and J. Shen, Comput. Phys. Commun. **108**, 147 (1998).